A STATISTICAL FRAMEWORK FOR THE CLASSIFICATION OF INFANT DT IMAGES

Mahmoud Mostapha[1], *Ahmed Soliman*[1], *Fahmi Khalifa*[1], *Ahmed Elnakib*[1]
Amir Alansary[1], *Matthew Nitzken*[1], *Manuel F. Casanova*[2] *and Ayman El-Baz*[1*]
[1]BioImaging Laboratory, Bioengineering Department, University of Louisville, Louisville, KY, USA.
[2]Department of Psychiatry and Behavioral Science, University of Louisville, Louisville, KY, USA.

ABSTRACT

This paper introduces a new adaptive atlas-based framework for the automated segmentation of different brain structures from infant diffusion tensor images (DTI). To model the brain images and their desired region maps, we used a joint Markov-Gibbs random field (MGRF) model that accounts for three image descriptors: (i) a 1^{st}-order visual appearance to describe the empirical distribution of DTI extracted features, (ii) an adaptive shape model, and (iii) a 3D spatially invariant 2^{nd}-order MGRF homogeneity descriptor. The 1^{st}-order visual appearance descriptor is accurately modeled using a linear combination of discrete Gaussians (LCDG) model having positive and negative components. The proposed adaptive shape model is constructed from a prior atlas database built using a subset of co-aligned training data sets that is adapted during the segmentation process guided by the visual appearance characteristics of several DTI features. To accurately account for the large inhomogeneity of infant brains, the homogeneity descriptor is modeled by a 2^{nd}-order translation and rotation invariant MGRF of region labels with analytically estimated potentials. The high accuracy of our segmentation approach was confirmed by testing it on 10 *in-vivo* infant DTI brain data sets using three metrics: the Dice similarity coefficient, the 95-percentile modified Hausdorff distance, and the absolute brain volume difference.

Index Terms— Infant, MGRF, LCDG, DTI Brain Segmentation

1. INTRODUCTION

Compared to the other imaging modalities, magnetic resonance imaging (MRI) has become today the most powerful and dominant non-invasive tool for clinical diagnosis of different brain diseases. Recently, an MRI technique known as diffusion tensor imaging (DTI) has been used to characterize the microstructural properties and macroscopic organization of white matter tissues in the brain [1]. DTI advantages over conventional MRI include its superior ability to reveal detailed anatomy of the white matter as DTI offers contrasts that are sensitive to fiber orientations. In addition, DTI delivers new insights about human brain connectivity, namely it provides a way to delineate abnormalities in specific connections in various pathological disorders [2]. DTI has a wide range of clinical applications; it is used to examine normative white matter development, neurodevelopmental disorders (e.g., autism), and neurodegenerative disorders (e.g., amyotrophic lateral sclerosis) [3]. Segmentation of anatomical structures such as white matter (WM), gray matter (GM), and cerebrospinal fluid (CSF) regions is an essential stage in any computer-aided diagnostic (CAD) system for brain diseases [4]. The tedious and time consuming nature of manual segmentation of the brain provided the drive for the development of several automated and semiautomated segmentation techniques.

Brain MRI segmentation meets with many challenges that stem from image noise, inhomogeneity, artifacts (e.g., partial volume effect), and boundary discontinuities due to the similarity in the visual appearance of adjacent brain structures. Moreover, the diffusion-sensitizing gradient used in diffusion weighted imaging (DWI) yields an amplification effect to the distortions that are related to patient motion [5]. This paper targets infant brain DTI segmentation that is more difficult than adult brain segmentation, which can be conducted using only the image intensity. Infant brains have a greatly reduced contrast, including a reverse in contrast in the WM and GM because of the immaturity of the brain tissues [6], and a higher amount of noise [7]. Furthermore, eddy current artifacts, and bulk motion distortions are additional difficulties that existed, especially in unsedated infants (see Fig. 1).

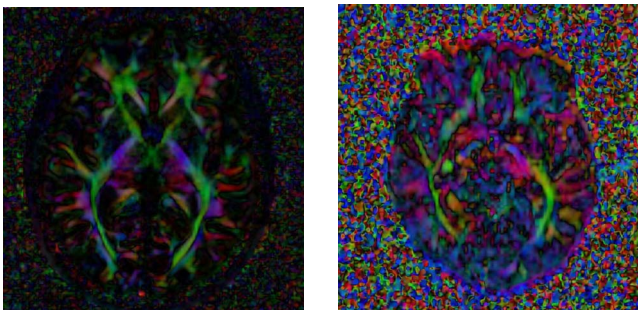

(a) (b)

Fig. 1. DTI-RGB map comparison for adult (a) and infant (b) brains.

Current techniques for brain DTI segmentation can be crudely classified into three main groups: (i) probabilistic and statistical based [8, 9], (ii) deformable model-based [10], and (iii) atlas-based techniques [11]. Most techniques mainly target adult brain segmentation, and limited techniques are fit for infant brain segmentation. Below, we will briefly overview some atlas-based techniques that target brain segmentation intended for studying infant brains with autism, which is the focus of this paper.

During the last few years, there have been numerous studies examining infant brains with autism, which use atlas-based techniques in the segmentation procedure. Wolff et al. [12], Elison et al. [13], and Neda et al. [14] introduced an atlas building procedure that contains two different registration frameworks using DTI and T2-weighted images. The intra-subject and inter-modality registrations were based on a multi-scale approach that employs both affine and B-spline transformations, using the normalized mutual information (MI) as a matching metric. Scans taken at different time intervals are linearly mapped to an atlas constructed from a patient at the

*Corresponding author:- Tel:(502)-852-5092, Fax:(502)-852-6806, E-mail: aselba01@louisville.edu

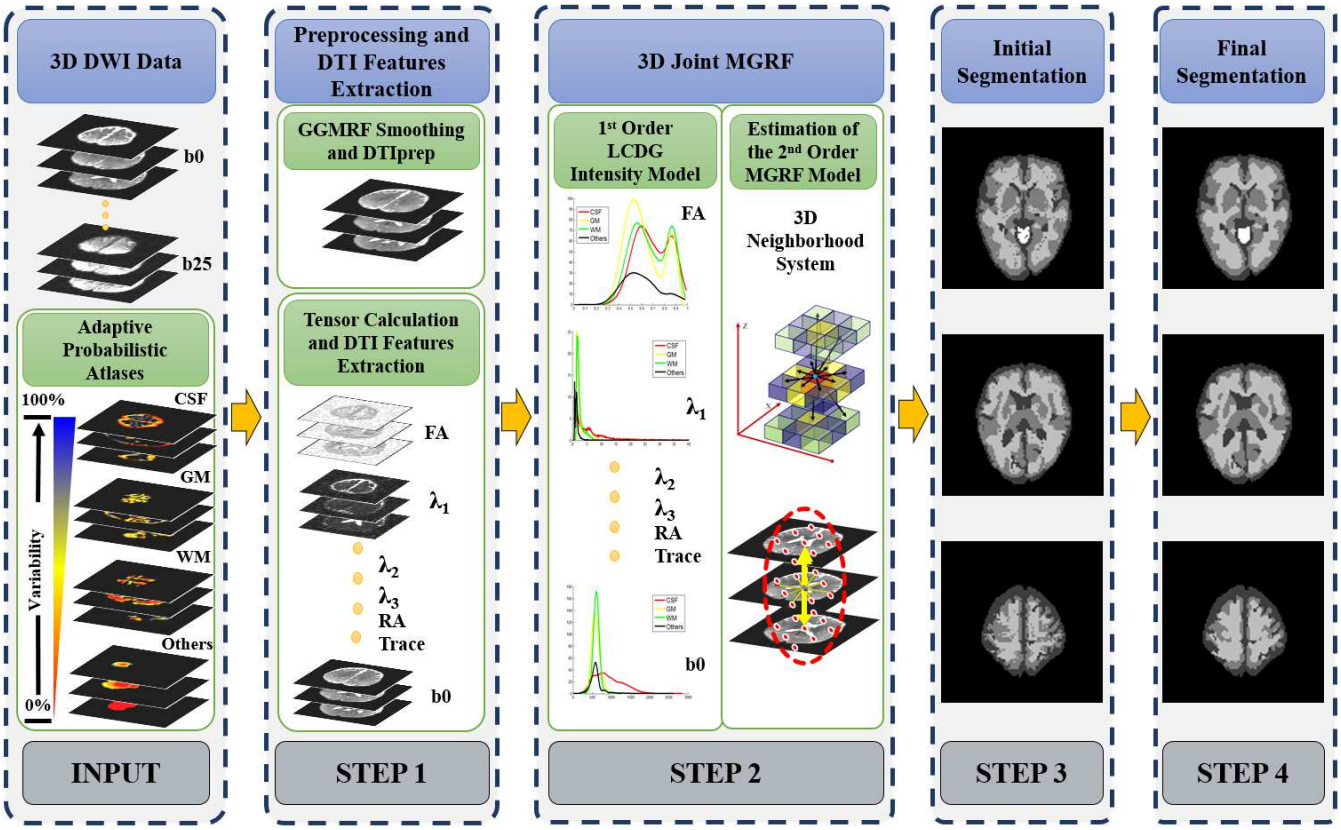

Fig. 2. The proposed segmentation framework.

age of one year. They are subsequently mapped using a nonlinear transformation to a T2-weighted atlas, and tensor images are estimated from the aligned DWI and averaged using the log-Euclidean method to produce a final DTI atlas.

To summarize, current DTI-based infant brain segmentation techniques suffer from the following limitations: (i) atlases constructed from multiple modalities (e.g., T2-weighted and DTI) will decrease the segmentation accuracy as a result of dissimilar contrast levels and inter-slice variability, and (ii) using nonlinear registration negatively affects the shape information, thus it prevents carrying out any shape-based statistical analysis on the segmented data, which could be beneficial in inspecting the relationship between WM and GM morphology [15]. Therefore, we propose a new atlas-based technique for the accurate segmentation of WM, GM, and CSF from DTI images (see Fig. 2), which will overcome the previously mentioned drawbacks. The proposed technique relies on a combination of adaptive probabilistic models for the shape (atlas) and current appearance features (1^{st}-order visual appearance and spatial interaction between brain voxels) [16]. These adaptive probabilistic models increase the segmentation accuracy by accounting for large inhomogeneities in infant brains and by reducing the effects of noise.

2. THE PROPOSED JOINT MGRF MODEL

Let $\mathbf{R} = \{(x, y, z) : 0 \leq x \leq X-1, 0 \leq y \leq Y-1, 0 \leq z \leq Z-1\}$; $\mathbf{Q} = \{0, 1, \ldots, Q-1\}$; and $\mathbf{L} = \{0, \ldots, L\}$ denote a finite 3D arithmetic lattice of the size of XYZ supporting grayscale images and their region (segmentation) maps, a finite set of Q integer gray values, and a set of region labels L, respectively. Let $\mathbf{g} = \{g_{x,y,z} : (x, y, z) \in \mathbf{R};\ g_{x,y,z} \in \mathbf{Q}\}$ and $\mathbf{m} = \{m_{x,y,z} : (x, y, z) \in \mathbf{R};\ m_{x,y,z} \in \mathbf{L}\}$ be a grayscale image taking values from $\mathbf{Q}$, i.e., $\mathbf{g} : \mathbf{R} \rightarrow \mathbf{Q}$, and a region map taking values from $\mathbf{L}$, i.e., $\mathbf{m} : \mathbf{R} \rightarrow \mathbf{L}$, respectively. An input brain image, $\mathbf{g}$, co-aligned to the training data base, and its map, $\mathbf{m}$, are described with a joint probability model: $P(\mathbf{g}, \mathbf{m}) = P(\mathbf{g}|\mathbf{m})P(\mathbf{m})$, which combines a conditional distribution of the images given the map $P(\mathbf{g}|\mathbf{m})$, and an unconditional probability distribution of maps $P(\mathbf{m}) = P_{\mathrm{sp}}(\mathbf{m})P_{\mathbf{V}}(\mathbf{m})$. Here, $P_{\mathrm{sp}}(\mathbf{m})$ denotes an adaptive shape prior, and $P_{\mathbf{V}}(\mathbf{m})$ is a Gibbs probability distribution with potentials $\mathbf{V}$, which specifies a Markov Gibbs random field (MGRF) model of spatially homogeneous maps $\mathbf{m}$. Details of the model's components are outlined below.

Adaptive Shape Model: In order to obtain a more accurate segmentation, we employed adaptive probabilistic atlases of the expected shapes of the different brain labels. To create the atlas database, a training set of images, collected for different subjects (10 data sets), are co-aligned by 3D affine transformations with 12 degrees of freedom in a way that maximizes their mutual information (MI) [17]. The probabilistic atlases are spatially variant independent random fields of region labels $P_{\mathrm{sp}}(\mathbf{m}) = \prod_{(x,y,z)\in\mathrm{R}} p_{\mathrm{sp}:x,y,z}(m_{x,y,z})$ for the co-aligned manually segmented data sets [18, 19], specified by voxel-wise empirical probabilities for each brain label $(p_{\mathrm{sp}:x,y,z}(l), l \in \{1, \ldots, L\})$. Based on the infant tissue probability maps provided by IDEA lab [20], we used the unified segmentation algorithm [21] implemented in statistical parametric mapping (SPM) software [22] to segment the non-diffusion (b0) scans of our training data sets. Then, an MR expert refined the generated initial segmentation to produce the final brain labels.

For each input DTI data to be segmented, the shape prior is constructed by an adaptive process guided by the visual appearance features of different brain structures in the b0 scan and six other DTI extracted features: the three eignvalues ($\lambda 1$, $\lambda 2$, and $\lambda 3$), fractional anisotropy (FA), relative anisotropy (RA), and Trace [2]. These six features are extracted from the tensor matrix generated for each DTI data set. In order to estimate the shape prior probabilities for each voxel in the test subject, we follow the steps summarized in Algorithm 1.

Algorithm 1 Key Steps for Creating the Adaptive Shape Model

1. Construct the atlas database through a co-alignment of the b0 scans, six other DTI extracted features , and manual segmentation of each of the preprocessed brains.
2. Use normalized cross correlation (NCC) to measure the similarity between the test subject and each subject in the atlas database, and choose the database subject that has the highest similarity to act as the reference in the registration process.
3. Register the test subject to the selected reference subject using 3D affine transformations with 12 degrees of freedom that maximizes their MI [17].
4. For each voxel in the test subject, calculate its shape prior probability according to the following steps:
   (a) Use the obtained transformation matrix (T) to transform each voxel to the atlas database domain.
   (b) Construct a 3D window with initial size of $N_{1i} \times N_{2i} \times N_{3i}$.
   (c) Search inside the window for voxels with corresponding grey level (b0 and six DTI features) in all training data sets.
   (d) If needed, increase the window size and redo the search until a non-empty result is found.
   (e) Create the labels probabilities based on the relative occurrence of each label from the search results.

1^{st}-Order Visual Appearance Descriptor: In addition to the learned adaptive prior descriptor, our approach accounts for the visual appearance of each brain structure in the b0 scan and six other DTI extracted features ($\lambda 1$, $\lambda 2$, $\lambda 3$, FA, RA, and Trace). The mixed empirical marginal 1D distribution of voxel intensities is separated into four individual components, associated with each label of the mixture. To model the current DTI appearance, the empirical distribution is precisely approximated with a linear combination of discrete Gaussians (LCDG) [23] with positive and negative components, which is based on a modified version of the classical Expectation-Maximization (EM) algorithm. The LCDG models the empirical distribution of the brain labels more accurately than a conventional mixture of only positive Gaussians. This yields a better initial region map that is formed by the voxel-wise classification of the image gray values.

Let $\mathbf{\Psi}_\theta = (\psi(q|\theta) : q \in \mathbf{Q})$ denote a discrete Gaussian (DG) with parameters $\theta = (\mu, \sigma)$, integrating a continuous 1D Gaussian density with mean μ and variance σ^2 over successive gray level intervals. The LCDG with four dominant positive DGs and $C_{\rm p} \geq 4$ positive and $C_{\rm n} \geq 0$ negative subordinate DGs is [23, 24]:

$$P_{\mathbf{w},\mathbf{\Theta}}(q) = \sum_{k=1}^{C_{\rm p}} w_{{\rm p}:k}\psi(q|\theta_{{\rm p}:k}) - \sum_{\kappa=1}^{C_{\rm n}} w_{{\rm n}:\kappa}\psi(q|\theta_{{\rm n}:\kappa})$$

where all the weights $\mathbf{w} = [w_{{\rm p}:k}, w_{{\rm n}:\kappa}]$ are non-negative and meet an obvious constraint $\sum_{k=1}^{C_{\rm p}} w_{{\rm p}:k} - \sum_{\kappa=1}^{C_{\rm n}} w_{{\rm n}:\kappa} = 1$. All LCDG parameters, including the DGs numbers, are estimated from the mixed empirical distribution to be modeled using the modified EM algorithm [23]. The complete LCDG model details are explained in [23].

3D Spatial Interaction MGRF Model: In order to perform a more accurate segmentation, spatially homogeneous 3D pair-wise interactions between the region labels are additionally incorporated in the model. These interactions are calculated using the popular Potts model (i.e., an MGRF with the nearest 26-neighbors of the voxels, as illustrated in Fig. 3), and analytic bi-valued Gibbs potentials that depend only on whether the nearest pairs of labels are equal or not. Let $f_{\rm eq}(\mathbf{m})$ denote the relative frequency of equal labels in the neighboring voxel pairs $((x,y,z),(x+\xi,y+\eta,z+\zeta)) \in \mathbf{R}^2; (\xi,\eta,\zeta) \in \{(\pm 1,0,0),(0,\pm 1,0),(\pm 1,\pm 1,0),(\pm 1,0,\pm 1),(0,\pm 1,\pm 1),(\pm 1,\pm 1,\pm 1)\}$. The initial region map results in an approximation with the following analytical maximum likelihood estimates of the potentials [25]: $v_{\rm eq} = -v_{\rm ne} \approx 2f_{\rm eq}(\mathbf{m}) - 1$, where $v_{\rm eq}$ and $v_{\rm ne}$ are the estimated potentials in the case of equal and non-equal labels, respectively. These estimates allow for computing the voxel-wise probabilities $p_{{\rm v}:x,y,z}(m_{x,y,z} = \lambda)$ of each brain label; $l \in \mathbf{L}$.

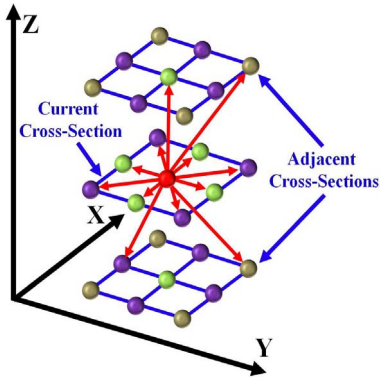

Fig. 3. Illustration of the 3D neighborhood system used.

One of the main advantages of the proposed approach is that in addition to the adaptive prior information, our approach depends on two other models (1^{st}-order and 2^{nd}-order visual appearance models) that are estimated directly from the input data, making our approach a complete adaptive segmentation tool. The complete steps of the proposed segmentation approach are summarized in Algorithm 2.

3. EXPERIMENTAL RESULTS

Performance assessment of the segmentation results were carried out through applying our technique on 54 diffusion weighted infant MR brain data sets obtained from the Infant Brain Imaging Study (IBIS) [29], and evaluated using 10 data sets with a manually segmented ground truth, obtained by an MR expert. Diffusion weighted MRI brain scans were obtained from a 3-T Siemens TIM Trio scanners (Siemens Medical Solutions, Malvern, PA.) using the following parameters: field of view of: 190 mm, number of slices: 75–81, a slice thickness: 2 mm, voxel resolution: $2 \times 2 \times 2$ mm^3, TR: 12,800–13,300 ms, TE: 102 ms, variable b values between 0 and 1,000 s/mm^2, 25 gradient directions, and a scan time of 5-6 minutes. The scans were obtained approximately at 6 months of age in infants with high risk of developing autism spectrum disorders (ASDs) [29].

The final goal of the proposed segmentation technique is to separate infant DTI brain images into four classes: WM, GM, CSF, and

Algorithm 2 Key Steps for the Proposed Segmentation Approach

1. Reduce DWI data inhomogeneities using a Generalized 3D Gauss-Markov random field (GGMRF) model [26].
2. Detect artifacts, correct motion and eddy current distortions and remove images with large artifacts using DTIprep software [27].
3. Derive DTI from DWI, and extract six DTI features ($\lambda 1$, $\lambda 2$, $\lambda 3$, FA, RA, and Trace) using 3D Slicer [28].
4. Approximate the marginal intensity distribution of the b0 scan and the six extracted DTI features using the LCDG model with four dominant modes.
5. Form an initial region map $\mathbf{m}$ using the marginal estimated density and prior adaptive shape of each label.
6. Find the Gibbs potentials for the MGRF model from the initial map [23].
7. Improve the region map $\mathbf{m}$ using voxel-wise Bayes classifier after integrating the three descriptors in the proposed joint MGRF model.

other brain tissues. A step-by-step of the proposed segmentation technique is demonstrated in Fig. 4. The input DTI data (Fig. 4(a)) is initially smoothed using the Generalized 3D Gauss-Markov random field (GGMRF) model [26] . Then, DTIprep software [27] is used to remove scan artifacts, and correct motion and eddy current distortions (Fig. 4 (b)). An initial segmentation is achieved using our constructed adaptive shape model and the marginal densities estimated from the b0 scan and the six DTI parameters (Fig. 4 (c)). To obtain the final segmentation, the initial results was refined using the proposed three descriptors (1^{st}-order visual appearance models, 3D spatial model, and adaptive shape model) as shown in Fig. 4(d).

The performance of the proposed segmentation framework was evaluated using three performance metrics: (i) the Dice similarity coefficient (DSC), (ii) the 95-percentile modified Hausdorff distance (MHD), and (iii) the percentage absolute volume difference (AVD) [30]. Metrics were computed by comparing a ground truth segmentation to results from the proposed segmentation technique. As demonstrated in Table 1, the DSC for segmentation of the WM, GM, and the CSF are 95.23$\pm$1.18%, 89.92$\pm$2.86%, and 87.96$\pm$3.31% , respectively, which confirms the high accuracy of the proposed segmentation techniques. Our experiments show that the proposed accurate identification of the joint MGRF model demonstrates promising results in segmenting GM and WM brain tissues from infant DTI images. Our present implementation in the C++ programming language on a Dell precession T7500 workstation (3.33Ghz Intel quad-core with 48GB RAM) takes about 8.1 ± 2.53 sec to process each test subject.

4. CONCLUSIONS

In conclusion, this paper proposed a new adaptive atlas-based framework for the automated segmentation of different brain structures from DTI. The proposed segmentation technique demonstrates that the integration of a 2^{nd}-Order MGRF spatial model with 1^{st}-Order visual appearance features is promising for controlling an adaptive shape model to segment DTI infant brains. The accuracy of the proposed segmentation framework can aid researchers to advance new methods that can help to distinguish between autistic and control infant brains.

In the future, we plan to further enhance our segmentation results by using nonnegative matrix factorization (NMF) [31] to extract meaningful features from a large dimensional feature space with attributes extracted from different DTI measurements. NMF will find the weights for each feature in order to create a feature space where different classes are more separable. Thanks to a continuing partnership between our group and the IBIS [29] group, there are plans to integrate the proposed approach into a CAD system for the early diagnosis of ASDs. The final developed segmentation framework will be integrated with other methodologies to explore features in the GM and WM regions of the brain.

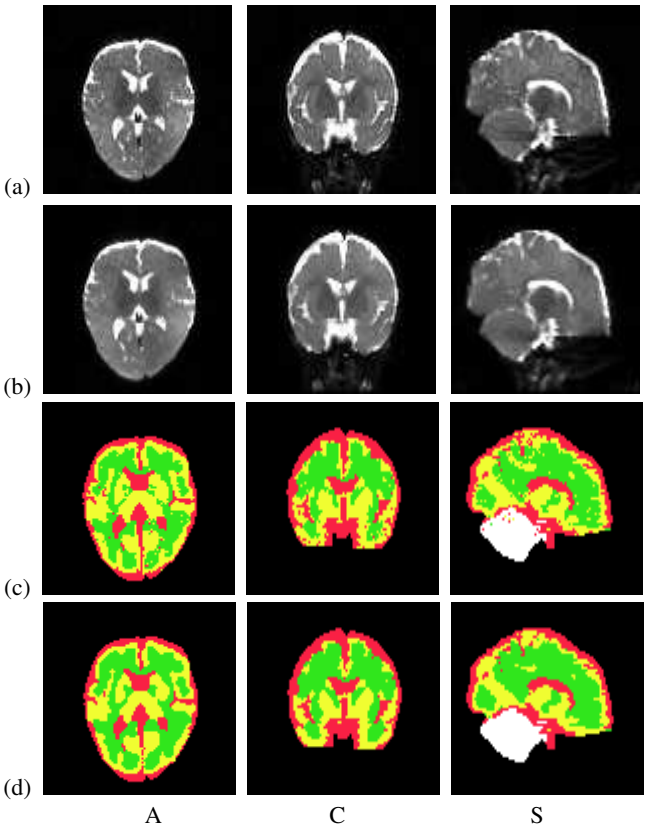

Fig. 4. Segmentation results of the proposed approach. The segmentation is performed in 3D, and the results are projected onto 2D axial (A), coronal (C), and sagittal (S) planes for visualization: (a) 2D profile of the original b0 scan images, (b) b0 scan images after MGRF smoothing and preprocessing using DTIprep [27], (c) initial segmentation using 1^{st}-order visual appearance models and adaptive shape model, and (d) final segmentation results using the proposed three models. Note that CSF, GM, WM, and other non-brain tissues are shown in red, yellow, green, and white, respectively.

Table 1. Accuracy of our segmentation.

Metric	CSF	GM	WM
DSC (%)	87.96$\pm$3.31	89.92$\pm$2.86	95.23$\pm$1.18
MHD (mm)	2.42$\pm$0.56	1.98$\pm$1.07	1.98$\pm$0.01
AVD (%)	6.10$\pm$4.70	9.85$\pm$2.34	5.15$\pm$2.03

References

[1] P. J. Basser, J. Mattiello, and D. LeBihan, "MR diffusion tensor spectroscopy and imaging," *Biophysical Journal*, vol. 66, no. 1, pp. 259–267, 1994.

[2] S. Mori and J.-D. Tournier, *Introduction to Diffusion Tensor Imaging 2e: And Higher Order Models*, Academic Press, 2013.

[3] Q. Dong, R. C. Welsh, T. L. Chenevert, R. C. Carlos, P. Maly-Sundgren, D. M. Gomez-Hassan, and S. K. Mukherji, "Clinical applications of diffusion tensor imaging," *Journal of Magnetic Resonance Imaging*, vol. 19, no. 1, pp. 6–18, 2004.

[4] H. Arimura, T. Magome, Y. Yamashita, and D. Yamamoto, "Computer-aided diagnosis systems for brain diseases in magnetic resonance images," *Algorithms*, vol. 2, no. 3, pp. 925–952, 2009.

[5] T. P. Trouard, Y. Sabharwal, M. I. Altbach, and A. F. Gmitro, "Analysis and comparison of motion-correction techniques in diffusion-weighted imaging," *Journal of Magnetic Resonance Imaging*, vol. 6, no. 6, pp. 925–935, 1996.

[6] H. Xue et al., "Automatic segmentation and reconstruction of the cortex from neonatal MRI," *Neuroimage*, vol. 38, no. 3, pp. 461–477, 2007.

[7] A. U. Mewes, P. S. Hueppi, H. Als, F. J. Rybicki, T. E. Inder, G. B. McAnulty, R. V. Mulkern, R. L. Robertson, M. J. Rivkin, and S. K. Warfield, "Regional brain development in serial magnetic resonance imaging of low-risk preterm infants," *Pediatrics*, vol. 118, no. 1, pp. 23–33, 2006.

[8] S. P. Awate, Z. Hui, and J. C. Gee, "A fuzzy, nonparametric segmentation framework for DTI and MRI analysis: With applications to DTI-tract extraction," *IEEE Transaction on Medical Imaging*, vol. 26, no. 11, pp. 1525–1536, 2007.

[9] Y. Wen, L. He, K. M. von Deneen, and Y. Lu, "Brain tissue classification based on DTI using an improved fuzzy c-means algorithm with spatial constraints," *Magnetic Resonance Imaging*, vol. 31, no. 9, pp. 1623–1630, 2013.

[10] L. Jonasson, P. Hagmann, C. Pollo, X. Bresson, C. Richero Wilson, R. Meuli, and J.-P. Thiran, "A level set method for segmentation of the thalamus and its nuclei in DT-MRI," *Signal Processing*, vol. 87, no. 2, pp. 309–321, 2007.

[11] U. Ziyan, M. R. Sabuncu, W. E. L. Grimson, and C.-F. Westin, "Consistency clustering: a robust algorithm for group-wise registration, segmentation and automatic atlas construction in diffusion MRI," *International Journal of Computer Vision*, vol. 85, no. 3, pp. 279–290, 2009.

[12] J. J. Wolff, H. Gu, G. Gerig, J. T. Elison, M. Styner, S. Gouttard, K. N. Botteron, S. R. Dager, G. Dawson, A. M. Estes, et al., "Differences in white matter fiber tract development present from 6 to 24 months in infants with autism.," *The American Journal of Psychiatry*, vol. 169, no. 6, pp. 589–600, 2012.

[13] J. T. Elison, S. J. Paterson, J. J. Wolff, J. S. Reznick, N. J. Sasson, H. Gu, K. N. Botteron, S. R. Dager, A. M. Estes, A. C. Evans, et al., "White matter microstructure and atypical visual orienting in 7-month-olds at risk for autism," *American Journal of Psychiatry*, 2013.

[14] N. Sadeghi, M. Prastawa, P. T. Fletcher, J. Wolff, J. H. Gilmore, and G. Gerig, "Regional characterization of longitudinal DT-MRI to study white matter maturation of the early developing brain," *Neuroimage*, 2012.

[15] P. Savadjiev, Y. Rathi, S. Bouix, A. R. Smith, R. T. Schultz, R. Verma, and C.-F. Westin, "Combining surface and fiber geometry: An integrated approach to brain morphology," in *Proceedings of Medical Image Computing and Computer-Assisted Intervention (MICCAI'13)*, pp. 50–57. 2013.

[16] M. Mostapha, A. Alansary, A. Soliman, F. Khalifa, M. Nitzken, R. Khodeir, M. F. Casanova, and A. El-Baz, "Atlas–based approach for the segmentation of infant dti mr brain images," in *Proceedings of IEEE International Symposium on Biomedical Imaging: From Nano to Macro (ISBI'14)*, 2014, pp. 1255–1258.

[17] P. A. Viola and W. M. W. III, "Alignment by maximization of mutual information," *International Journal on Computer Vision*, vol. 24, no. 2, pp. 137–154, 1997.

[18] F. Khalifa, A. El-Baz, G. Gimel'farb, and M. A. El-Ghar, "Non-invasive image-based approach for early detection of acute renal rejection," in *Proceedings of Medical Image Computing and Computer-Assisted Intervention (MICCAI'10)*, 2010, pp. 10–18.

[19] F. Khalifa, G. M. Beache, M. Abou El-Ghar, T. El-Diasty, G. Gimel'farb, M. Kong, and A. El-Baz, "Dynamic contrast-enhanced MRI-based early detection of acute renal transplant rejection," *IEEE Transactions on Medical Imaging*, vol. 32, no. 10, pp. 1910–1927, 2013.

[20] F. Shi, P.-T. Yap, G. Wu, H. Jia, J. H. Gilmore, W. Lin, and D. Shen, "Infant brain atlases from neonates to 1-and 2-year-olds," *PLoS One*, vol. 6, no. 4, pp. e18746, 2011.

[21] J. Ashburner and K. J. Friston, "Unified segmentation," *Neuroimage*, vol. 26, no. 3, pp. 839–851, 2005.

[22] Statistical Parametric Mapping (SPM), ," `http://www.fil.ion.ucl.ac.uk/spm/`.

[23] A. Farag, A. El-Baz, and G. Gimel'farb, "Precise segmentation of multimodal images," *IEEE Transaction on Image Processsssing*, vol. 15, no. 4, pp. 952–968, 2006.

[24] A. El-Baz, A. Elnakib, F. Khalifa, M. A. El-Ghar, P. McClure, A. Soliman, and G. Gimel'farb, "Precise segmentation of 3-D magnetic resonance angiography," *IEEE Transaction on Biomedical Engineering*, vol. 59, no. 7, pp. 2019–2029, 2012.

[25] A. El-Baz, *Novel stochastic models for medical image analysis*, Ph.D. thesis, University of Louisville, Louisville, KY, USA, 2006.

[26] C. Bouman and K. Sauer, "A generalized gaussian image model for edge-preserving MAP estimation," *IEEE Transaction on Image Processsssing*, vol. 2, pp. 296–310, 1993.

[27] Z. Liu, Y. Wang, G. Gerig, S. Gouttard, R. Tao, T. Fletcher, and M. Styner, "Quality control of diffusion weighted images," in *Proceedings of SPIE Medical Imaging 2000: Image Processing (SPIE'10)*, 2010, pp. 76280J–76280J.

[28] A. Fedorov, R. Beichel, J. Kalpathy-Cramer, J. Finet, J.-C. Fillion-Robin, S. Pujol, C. Bauer, D. Jennings, F. Fennessy, M. Sonka, et al., "3D slicer as an image computing platform for the quantitative imaging network," *Multidisciplinary Respiratory Medicine*, vol. 30, no. 9, pp. 1323–1341, 2012.

[29] Infant Brain Imaging Study (IBIS), ," `http://www.ibisnetwork.org/`.

[30] K. O. Babalola, B. Patenaude, P. Aljabar, J. Schnabel, D. Kennedy, W. Crum, S. Smith, T. Cootes, M. Jenkinson, and D. Rueckert, "An evaluation of four automatic methods of segmenting the subcortical structures in the brain," *Neuroimage*, vol. 47, no. 4, pp. 1435–1447, 2009.

[31] D. D. Lee and H. S. Seung, "Learning the parts of objects by non-negative matrix factorization," *Nature*, vol. 401, no. 6755, pp. 788–791, 1999.